THE JOURNAL OF BIOLOGICAL CHEMISTRY VOL. 285, NO. 3, pp. 1809–1821, January 15, 2010

A Synthetic Combinatorial Strategy for Developing α-Conotoxin Analogs as Potent α_7 Nicotinic Acetylcholine Receptor Antagonists*[S]

Received for publication, October 7, 2009, and in revised form, November 5, 2009 Published, JBC Papers in Press, November 9, 2009, DOI 10.1074/jbc.M109.071183

Christopher J. Armishaw[‡1], Narender Singh[‡], Jose L. Medina-Franco[‡], Richard J. Clark[§2], Krystle C. M. Scott[‡], Richard A. Houghten[‡], and Anders A. Jensen[¶3]

From the [‡]Torrey Pines Institute for Molecular Studies, Port St. Lucie, Florida 34987, the [§]Institute for Molecular Bioscience, University of Queensland, Brisbane, Queensland 4072, Australia, and the [¶]Department of Medicinal Chemistry, Faculty of Pharmaceutical Sciences, University of Copenhagen, 2100 Copenhagen, Denmark

α-Conotoxins are peptide neurotoxins isolated from venomous cone snails that display exquisite selectivity for different subtypes of nicotinic acetylcholine receptors (nAChR). They are valuable research tools that have profound implications in the discovery of new drugs for a myriad of neuropharmacological conditions. They are characterized by a conserved two-disulfide bond framework, which gives rise to two intervening loops of extensively mutated amino acids that determine their selectivity for different nAChR subtypes. We have used a multistep synthetic combinatorial approach using α-conotoxin ImI to develop potent and selective α_7 nAChR antagonists. A positional scan synthetic combinatorial library was constructed based on the three residues of the *n*-loop of α-conotoxin ImI to give a total of 10,648 possible combinations that were screened for functional activity in an α_7 nAChR Fluo-4/Ca^{2+} assay, allowing amino acids that confer antagonistic activity for this receptor to be identified. A second series of individual α-conotoxin analogs based on the combinations of defined active amino acid residues from positional scan synthetic combinatorial library screening data were synthesized. Several analogs exhibited significantly improved antagonist activity for the α_7 nAChR compared with WT-ImI. Binding interactions between the analogs and the α_7 nAChR were explored using a homology model of the amino-terminal domain based on a crystal structure of an acetylcholine-binding protein. Finally, a third series of refined analogs was synthesized based on modeling studies, which led to several analogs with refined pharmacological properties. Of the 96 individual α-conotoxin analogs synthesized, three displayed ≥10-fold increases in antagonist potency compared with WT-ImI.

Venomous marine cone snails continue to provide researchers with a valuable source of ligands able to pharmacologically distinguish between various classes of ion channels and receptors (1). Their venom is used to swiftly immobilize their fast moving prey, a result of the singular and combined actions of between 50 and 200 individual peptide neurotoxin components known as conotoxins. Conotoxins are gene-encoded products that are expressed in venom glands as natural combinatorial peptide libraries (2). It is estimated that across the 500 species that make up entire genus of cone snails, there are more than 100,000 individual conotoxins with unique neuropharmacological properties (3).

Nicotinic acetylcholine receptors (nAChRs)[4] are ligand-gated ion channels that mediate the fast excitatory cholinergenic neurotransmission in the central and peripheral nervous systems (4). They are involved in cognitive function, pain pathways, and nicotine reward mechanisms (5). They are pentameric complexes composed of five closely related subunits arranged around a central cation conducting pore. The subunits are divided into the α_1, β_1, γ, and δ/ε subunits forming the muscle-type nAChRs and the α_2–α_{10} and β_2–β_4 subunits forming neuronal nAChRs (6). Each nAChR subtype is characterized by distinct pharmacological properties and is involved in a range of physiological and pathophysiological functions. For example, α_7 nAChRs are believed to play an important role in learning and memory; hence they have been proposed to be involved in diseases such as schizophrenia and Alzheimer disease (5). The large number of physiologically relevant nAChR subtypes and the numerous diverse physiological functions regulated by them underlines the importance of developing ligands that can specifically target different subtypes of these receptors.

α-Conotoxins are selective antagonists for different subtypes of nAChRs (7). They typically contain 12–20 amino acid residues and consist of two highly conserved disulfide bonds connected via a [1–3],[2–4] (globular) arrangement, giving rise to a two-loop cysteine framework, denoted *m* and *n*, respectively

* This work was supported in part by the State of Florida and the Arthritis and Chronic Pain Research Institute.

[S] The on-line version of this article (available at http://www.jbc.org) contains supplemental Figs. S1 and S2 and Tables S1 and S2.

The structural data have been deposited in the Biological Magnetic Resonance Bank under BMRB code 20107.

[1] To whom correspondence should be addressed: Torrey Pines Institute for Molecular Studies, 11350 SW Village Pkwy., Port St. Lucie, FL 34987. Tel.: 772-345-4720; Fax: 772-345-3649; E-mail: carmishaw@tpims.org.

[2] National Health and Medical Research Council career development award fellow.

[3] Supported by the Danish Medical Research Council and the Lundbeck Foundation.

[4] The abbreviations used are: nAChR, nicotinic acetylcholine receptor; Abu, α-aminobutyric acid; AChBP, acetylcholine-binding protein; Aph, 4-aminophenylalanine; Boc, *tert*-butyloxycarbonyl; Cha, cyclohexylalanine; Dmt, 2,6 dimethyltyrosine; Mty, *O*-methyltyrosine; Nal, 1-naphthylalanine; Nph, 4-nitrophenylalanine; Nva, norvaline; PS-SCL, positional scanning synthetic combinatorial library; Pyr, 3-pyridinylalanine; RP-HPLC, reverse-phase-high pressure liquid chromatography.

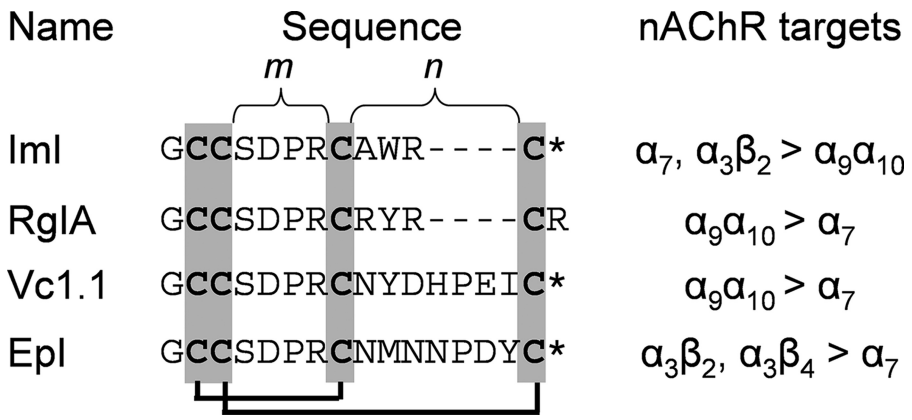

FIGURE 1. **Sequences of selected α-conotoxins containing the SDPR motif in the *m*-loop.** *Asterisk* denotes a carboxyl-terminal carboxamide. Cysteine residues are shaded in *gray*, and the native disulfide bond connectivity is indicated.

(Fig. 1). With the exception of the conserved cysteines, each position in the α-conotoxin sequence is extensively mutated. The variability of amino acids and functionalities contained within the loops has been shown to determine the potency and subtype selectivity profile for the nAChRs (8–16). The published x-ray co-crystal structures of several α-conotoxins in complex with acetylcholine-binding proteins (AChBPs) have been reported, providing structural insight into α-conotoxin/nAChR binding at the molecular level (17–20). AChBPs are a class of water-soluble proteins that display significant sequence homology with the ligand-binding domain of α_7 nAChRs. These co-crystal structures have been used to yield several new α-conotoxin analogs characterized by even more potent antagonist activities and different selectivity profiles than the native toxins (14).

The α4/3-conotoxins are a rich source of functionally diverse inhibitors of all α-subunit-containing nAChRs (21). Several examples, including α-conotoxins ImI, ImII, and RgIA, that target the α_7 and $\alpha_9\alpha_{10}$ nAChRs are well characterized, and more are continually being discovered (22). Interestingly, ImI and RgIA differ by only three residues and share an SDPR *m*-loop sequence, with variability occurring in the *n*-loop (Fig. 1). However, ImI and RgIA are selective for the α_7 and $\alpha_9\alpha_{10}$ nAChRs, respectively. Furthermore, the SDPR *m*-loop motif is also found in the α4/7-conotoxins EpI and Vc1.1, and it has been suggested that the α4/3-conotoxin *n*-loop residues may be important for refining nAChR selectivity (21).

Given that conotoxins are traditionally discovered from cone snail venom extracts that are themselves the natural combinatorial mixtures of bioactive peptides, it occurred to us that synthetic mixture-based combinatorial libraries of conotoxin would be of value in structure-activity relationship studies. With their highly conserved cysteine frameworks and intervening loops of hypermutated amino acids that gives rise to rigid three-dimensional conformations, conotoxins represent attractive combinatorial templates. Positional scanning synthetic combinatorial libraries (PS-SCL) are mixture-based libraries that provide a rapid means to acquire information regarding all possible variable positions within a chemical framework (23–25). They contain both defined and mixture positions of diversity, enabling the most active functionalities for each position to be identified directly from initial screening data, allowing the design of individual compounds (24, 26–28).

In this study, we have developed novel ligands for the α_7 nAChR using a multistep synthetic combinatorial approach through modification of the three residues forming the *n*-loop of α-conotoxin ImI. We have also employed homology modeling and docking studies using the ImI-AChBP complex to rationalize observed differences in antagonist potency and to refine the pharmacological properties of these analogs.

EXPERIMENTAL PROCEDURES

Peptide Synthesis—All peptides were assembled by solid-phase peptide synthesis using 2.5 × 2.5-cm polypropylene tea bags (29), each containing 100 mg of 4-methylbenzhydrylamine resin (ChemImpex, Wood Dale, IL). Couplings were performed using a modified *tert*-butyloxycarbonyl (Boc)/2-(1*H*-benzotriazol-1-yl)-1,1,3,3-tetramethyluronium hexafluorophosphate with an *in situ* neutralization procedure (30). *X*-positions were coupled as mixtures of N^{α}-Boc protected amino acids using adjusted concentration ratios to compensate for the relative reaction rates in competitive couplings (31). Following assembly, the tea bags were treated with 30% piperidine; the N^{α}-Boc protecting group was removed, neutralized, and pretreated with low-HF (25% HF, 60% dimethylsulfide, 10% *p*-cresol, 5% 1,2-ethanedithiol) for 2 h at 0 °C. Peptides were cleaved from the resin using HF/*p*-cresol/*p*-thiocresol (18:1:1) for 2 h at 0 °C. The HF was evaporated under a stream of nitrogen, precipitated with cold diethyl ether, and lyophilized. Analytical liquid chromatography-mass spectrometry confirmed the purity and molecular mass of individually synthesized peptides.

Crude samples were individually oxidized by gently agitating in a solution of 0.1 M ammonium bicarbonate, 50% isopropyl alcohol, pH 8.2, for 2 days at room temperature in an open vessel. PS-SCL mixtures were injected onto a preparative C_{18} RP-HPLC column and eluted from isocratic 62% acetonitrile followed by lyophilization to remove associated buffer salts and residual scavengers. Individual analogs were eluted from a linear gradient of water/acetonitrile (2–62% for 30 min) containing 0.1% trifluoroacetic acid and fractionated accordingly. Regioselective synthesis of compound 36 (globular and ribbon isomers) was achieved by stirring the reduced/*S*-acetomidomethyl-protected peptide in 0.1 M NH_4HCO_3 for 2 days, and isolating by preparative RP-HPLC. The partially oxidized peptides (~10 mg) were dissolved in 80% methanol (25 ml), and 0.1 M HCl was added (1 ml), followed by 0.1 M I_2 in methanol (2.5 ml). The solution was stirred for 10 min before quenching with 0.1 M sodium thiosulfate. The fully oxidized peptides were finally isolated using preparative RP-HPLC.

NMR Spectroscopy—NMR data were recorded on a sample dissolved in 90% H_2O, 10% D_2O at pH 3.5 using a Bruker ARX

600 MHz spectrometer. Two-dimensional total correlation spectroscopy and nuclear Overhauser effect spectroscopy NMR were acquired for all compounds, and additional DQF-COSY and E-COSY experiments were recorded for compound 36. For compound 36, peak intensities from a nuclear Overhauser effect spectroscopy spectrum with a mixing time of 200 ms at 285 K were used to determine distance restraints. Backbone dihedral restraints were determined from $^3J_{\mathrm{HN\text{-}H}\alpha}$ coupling constants, and ϕ angles were restrained to $-60 \pm 30°$ for $^3J_{\mathrm{HN\text{-}H}\alpha} < 5.8$ Hz (Cys^2, Cys^3, Asp^5, Tyr^{10}, and Cys^{12}), $-120 \pm 30°$ for $^3J_{\mathrm{HN\text{-}H}\alpha} > 8.0$ Hz (Abu11), and $-100 \pm 80°$ when $H_{\alpha i-1} - HN_i$ is significantly stronger than $H_{\alpha i-1} - HN_i$ (Ser^4 and Leu^9). Intra-residue nuclear Overhauser effect and $^3J_{\mathrm{HN\text{-}H}\beta}$ coupling patterns were used in assigning χ^1 angle restraints of some side chains (Cys^2, Cys^3, Ser^4, Arg^7, and Cys^8 to $180 \pm 30°$ and Cys^{12} to $-60 \pm 30°$).

Initial structures were generated using Cyana software (32), and the final structure calculations were performed using a simulated annealing protocol with CNS (33) as described previously (34). Fifty structures were calculated, and the 20 structures with the lowest overall energies were retained for analysis. Structures were visualized using MOLMOL (35) and analyzed with PROMOTIF (36) and PROCHECK_NMR (37).

Pharmacology—α-Conotoxin analogs were functionally characterized at the α_7 nAChR in the fluorescence-based Fluo-4/Ca^{2+} assay using a stable α_7-GH3 cell line (38) as described previously (14). Cell lines were split into poly-D-lysine-coated black 96-well clear bottom plates (BD Biosciences), following a 64–72-h incubation. On the day of the assay, the culture medium was aspirated, and the cells were incubated in 50 μl of assay buffer (Hanks' buffered saline solution containing 20 mM HEPES, 1 mM $CaCl_2$, 1 mM $MgCl_2$, and 2.5 mM probenecid, pH 7.4) supplemented with 6 mM Fluo-4/AM (Molecular Probes, Eugene, OR) at 37 °C for 1 h. The buffer was aspirated, and the cells were washed once with 100 μl of assay buffer, followed by addition of 100 μl of assay buffer supplemented with 100 μM genistein and various concentrations of the α-conotoxin analogs. Following 30 min of incubation at 37 °C in a 5% CO_2 incubator, the 96-well plate was assayed in a NOVOstar™ microplate reader (BMG Labtechnologies, Offenburg, Germany) measuring emission at 520 nm caused by excitation at 485 nm before and up to 60 s after addition of 33 μl of agonist solution in assay buffer. The compounds were characterized in duplicate at least three times using EC_{80}–EC_{90} concentrations of acetylcholine as agonist.

Selected α-conotoxin analogs were also functionally characterized at a HEK293 cell line stably expressing the rat $\alpha_3\beta_4$ nAChR and at a HEK293T cell line stably expressing the mouse $\alpha_4\beta_2$ nAChR (39, 40). The characterization at the $\alpha_3\beta_4$-HEK293 cell line was performed in the Fluo-4/Ca^{2+} assay. This assay was performed essentially as described for the α_7-GH3 cell line, except that genistein was not included in the assay buffer and EC_{80}–EC_{90} concentrations of epibatidine, not acetylcholine, were used as agonist. The characterization at the $\alpha_4\beta_2$-HEK293 cell line was performed in the Fluorescent Imaging Plate Reader Membrane Potential Blue™ assay (Molecular Devices) as described previously, using EC_{80}–EC_{90} concentrations of epibatidine as agonist (14).

Homology Modeling and Molecular Dynamics—A homology model of the extracellular amino-terminal domain of human nAChR α_7 was built using the *Aplysia* AChBP x-ray crystal structure bound with ImI (Protein Data Bank code 2BYP (19)). Sequence alignment of nAChR and AChBP was performed through ClustalW (41) and Prime; a protein structure prediction suite from Schrödinger LLC was used for model building (42). The aligned sequence of query and template showed 26% homology and 67% similarity. A homology structure was built using this aligned template taking into account the effects of solvent and the bound conotoxin through the various algorithms implemented in Prime. Missing query residues that did not match or align well with the template sequence were built using an *ab initio* procedure (43). Water molecules were retained from the template, and all the steric clashes were refined through minimization using OPLS2005 force field. The final model showed a backbone root mean square deviation of 0.49 Å with the template structure. Using this model, two separate docking models were generated using high and low affinity binding analogs from the second series of compounds. In both of these models, the pentameric nAChR structure was retained, superimposed from the template structure, and mutated according to the second iteration library α_7 nAChR functional assays. In model 1, ImI was mutated to Leu-Trp-Abu (compound 28, *high* antagonist potency analog), and in model 2 ImI was mutated to Ala-Phe-Arg (compound 5, *low* antagonist potency analog).

To further refine the docked complexes, short 500-ps Molecular Dynamics simulations were performed using the NAMD2 program (44) with the CHARMM 29b2 force field (45). The initial docked and refined structures from the previous step were taken as starting points for Molecular Dynamics simulations. The system setup procedure was initiated by adding hydrogen atoms and a box of TIP3 water molecules (solvation), such that there was at minimum 13.0 Å of water between the surface of the protein and the edge of the simulation box using the Solvate plug-in of the Visual Molecular Dynamics program (46). Any added bulk water molecules within 2.5 Å of the protein were excluded. To maintain the electrical neutrality of the system, appropriate numbers of ions (15 Na^+) were added using the Autoionize plug-in in Visual Molecular Dynamics programs, which were initially set at least 7.0 Å away from the surface of the protein.

RESULTS

Construction of PS-SCL

An initial PS-SCL based on the three residues in the α-conotoxin ImI *n*-loop was constructed to identify amino acid substitutions in this loop that confer activity for the α_7 nAChR. Three sub-libraries were prepared, where O_n is a single defined position, and *X* is an equimolar mixture of 22 natural and non-natural L-amino acids (see Table 1). A total of 66 mixtures, each containing 484 compounds, were obtained in three sub-libraries consisting of a total of 10,648 possible individual conotoxins. Cysteine was omitted from the O_n and *X*-positions to avoid interfering with the conserved disulfide bond framework during oxidative folding. Methionine was also omitted from the

TABLE 1

Functional characteristics of the α-conotoxin ImI PS-SCL at the α_7-GH3 cell line in the Fluo-4/Ca^{2+} assay

The data are the means of 3–5 individual experiments performed in duplicate. EC_{80}–EC_{90} concentrations of acetylcholine were used for the experiments.

Amino acid	O_9		O_{10}		O_{11}	
	IC_{50}	$-\log_{10}[IC_{50}] \pm$ S.E.	IC_{50}	$-\log_{10}[IC_{50}] \pm$ S.E.	IC_{50}	$-\log_{10}[IC_{50}] \pm$ S.E.
	μM		μM		μM	
WT-ImI	2.0	5.70 ± 0.04				
Ala	21	4.67 ± 0.02	20	4.69 ± 0.05	16	4.80 ± 0.01
Asp	>100	<4.0	25	4.60 ± 0.04	~50	~4.3
Glu	~100	~4.0	>100	<4.0	23	4.63 ± 0.04
Phe	~50	~4.3	7.9	5.10 ± 0.04	25	4.60 ± 0.04
Gly	~50	~4.3	17	4.76 ± 0.04	22	4.65 ± 0.03
His	9.8	5.01 ± 0.02	18	4.75 ± 0.05	6.6	5.18 ± 0.02
Ile	9.5	5.02 ± 0.05	11	4.95 ± 0.04	23	4.64 ± 0.02
Lys	19	4.72 ± 0.05	~50	~4.3	24	4.61 ± 0.03
Leu	8.7	5.06 ± 0.04	19	4.73 ± 0.03	20	4.70 ± 0.03
Nle	11	4.96 ± 0.03	13	4.87 ± 0.05	19	4.73 ± 0.03
Asn	~50	~4.3	~50	~4.3	15	4.82 ± 0.03
Pro	18	4.75 ± 0.05	~100	~4.0	23	4.64 ± 0.03
Gln	~50	~4.3	~50	~4.3	21	4.67 ± 0.03
Arg	20	4.69 ± 0.02	~50	~4.3	20	4.69 ± 0.03
Ser	50	~4.3	16	4.80 ± 0.02	18	4.74 ± 0.03
Thr	~100	~4.0	~50	~4.3	20	4.69 ± 0.05
Val	11	4.95 ± 0.02	29	4.54 ± 0.01	13	4.90 ± 0.04
Trp	13	4.89 ± 0.05	4.8	5.32 ± 0.03	7.8	5.11 ± 0.03
Tyr	30	4.52 ± 0.02	9.3	5.03 ± 0.03	12	4.93 ± 0.05
Abu	19	4.71 ± 0.03	~50	~4.3	12	4.92 ± 0.04
Hyp	~50	~4.3	~100	~4.0	18	4.75 ± 0.05
Nva	2.4	5.62 ± 0.03	32	4.49 ± 0.02	19	4.73 ± 0.04

library to avoid complications associated with the formation of its corresponding methionine sulfoxide. As such, isosteric Abu and norleucine were included on the O_n- and *X*-positions, together with Nva to complete the series of side chains containing hydrophobic alkyl groups. Additionally, hydroxyproline, a commonly occurring post-translational modification found in several conotoxins, was also incorporated into this library.

The PS-SCL was assembled using manual solid-phase peptide synthesis with Boc chemistry using polypropylene tea bags (29). *X*-positions were coupled using the portioning mixing strategy, which greatly simplifies library assembly compared with other approaches such as divide-couple-recombine or split syntheses (25). However, competitive coupling rates can be predominantly influenced by the relative nucleophilicity and steric hindrance of the incoming activated amino acid. Therefore, predetermined ratios were used by adjusting the relative concentration of each amino acid in the *X*-position (31).

Following assembly of the PS-SCL, each sample was cleaved using a two-step low-high HF procedure. Each sample was oxidized as a crude mixture in aqueous buffer consisting of 0.1 M NH_4HCO_3, pH 8.2, containing 50% isopropyl alcohol, which has been reported as the optimum condition for generating the native disulfide bond isomer of WT-ImI (47), and subsequently isolated from the oxidation buffer by elution with 62% isocratic acetonitrile on preparative RP-HPLC.

Functional Characterization of Mixture-based Libraries

The PS-SCL mixtures were screened for inhibitory α_7 nAChR signaling in α_7-GH3 cells using the Fluo-4/Ca^{2+} assay (Table 1 and Fig. 2) (38). We and others have previously found that that the α_7 nAChR in this and other fluorescence-based functional assays displays functional properties that are in agreement with reported electrophysiological recordings (38, 48).

Screening and deconvolution of the PS-SCL library revealed information regarding amino acid residues in positions O_9, O_{10}, and O_{11} in WT-ImI for optimal binding to the α_7 nAChR. In the case of the O_9-position, the most active amino acid was defined as Nva, since this mixture exhibited a similar IC_{50} value to WT-ImI ($IC_{50}^{WT\text{-}ImI}/IC_{50}^{PS\text{-}SCL}$ ratio 0.82). Introduction of Leu and Ile residues in position O_9 also resulted in mixtures with high antagonist potencies, displaying $IC_{50}^{WT\text{-}ImI}/IC_{50}^{PS\text{-}SCL}$ ratios of 0.23 and 0.21, respectively. Notably, each of these three mixtures exhibited significantly higher antagonist potencies than the mixtures containing the Ala residue also present in this position in WT-ImI ($IC_{50}^{WT\text{-}ImI}/IC_{50}^{PS\text{-}SCL}$ ratio 0.10). In contrast, the most active amino acid at the O_{10}-position was the Trp residue also found in WT-ImI ($IC_{50}^{WT\text{-}ImI}/IC_{50}^{PS\text{-}SCL}$ ratio 0.43). Other residues introduced at the O_{10}-position, which gave rise to mixtures with high antagonist potencies, were the other aromatic side chain bearing amino acids Phe and Tyr ($IC_{50}^{WT\text{-}ImI}/IC_{50}^{PS\text{-}SCL}$ ratios 0.25 and 0.23, respectively). Finally, in the O_{11}-position, the PS-SCL mixture with the Arg residue, also found in this position in WT-ImI, exhibited weaker antagonist activity ($IC_{50}^{WT\text{-}ImI}/IC_{50}^{PS\text{-}SCL}$ ratio 0.10) compared with mixtures with His (ratio 0.30) and Trp (ratio 0.25), followed by mixtures with Abu and Tyr (both ratios of 0.16). To this end, deconvolution of the PS-SCL, including native WT-ImI residues, involved choosing Ala, Nva, and Leu residues in the O_9-position, Trp, Phe, and Tyr residues in the O_{10}-position, and Abu, Arg, His, and Trp residues in the O_{11}-position.

Construction and Functional Characterization of a Second Iteration Library of Individual Analogs

Combinations of the residues giving rise to the most potent PS-SCL mixtures were used to construct a second series library consisting of a total of 36 individual analogs (see Table 2). Although oxidation using 0.1 M NH_4HCO_3, 50% isopropyl alco-

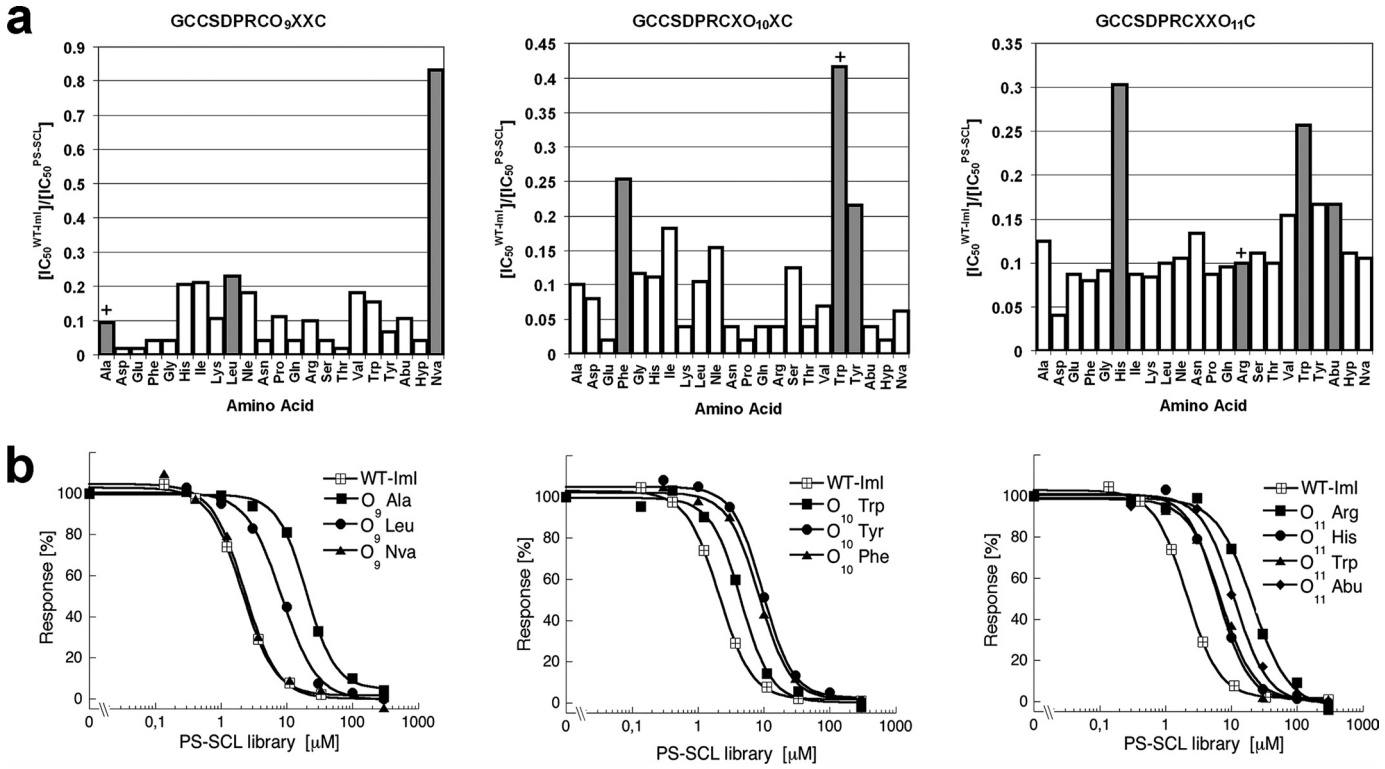

FIGURE 2. **Functional characterization of α-conotoxin ImI PS-SCL mixtures at the α_7-GH3 cell line in the Fluo-4/Ca^{2+} assay.** *a,* each *graph* shows the results of one of the three sub-libraries, with *bars* representing the ratio of the IC_{50} values of each mixture relative to WT-ImI. The specific IC_{50} values determined for the mixtures are given in supplemental Table S1. *Bars* marked with + indicate mixtures with the native amino acids at the O_n-position. *Bars* shown in *gray* represent amino acid substitutions that were used to construct a second series of individual analogs. *b,* concentration-response curves of WT-ImI and selected PS-SCL mixtures using EC_{80}–EC_{90} concentrations of acetylcholine as agonist. The figures depict data from single representative experiments, and *error bars* are omitted for reasons of clarity.

hol yielded one major isomer as determined by LC/MS, several analogs were accompanied by a second minor peak with identical mass (~10% of the total yield of oxidized conotoxin). This was presumably the ribbon isomer (*i.e.* [1–4],[2–3] disulfide bond connectivity) and in all cases was readily separated using preparative RP-HPLC.

The individual analogs were tested for activity at the α_7 nAChR in the Fluo-4/Ca^{2+} assay (Table 2 and Fig. 3*a*). Individual analogs are defined in this study as being *very high* (>10-fold increase compared with that of WT-ImI), high (6–10-fold increase), *medium* (0–6-fold increase), low (10-fold decrease) antagonist potency, or *inactive* (>10-fold decrease).

For single amino acid substitutions in WT-ImI, nearly all analogs containing an Ala residue at O_9 displayed low antagonist potencies at the α_7 nAChR (Table 2 and Fig. 3*a*), with compounds 5, 8, 11, and 12 displaying no significant activity. Compounds 2 and 10 were the only analogs containing the native Ala at position O_9 that exhibited similar antagonist potency to WT-ImI. Although a considerable number of the compounds containing Nva and Leu at O_9 clearly showed increased activity, the analogs with single substitutions of Ala for Nva or Leu in WT-ImI (compounds 13 and 25) both displayed IC_{50} values comparable with WT-ImI. The analog containing single amino acid substitutions at O_{10} with Tyr (compound 9) exhibited a 5-fold lower antagonist potency compared with WT-ImI, whereas substitution with Phe (compound 5) was inactive. At O_{11}, substitution of Arg^{11} for His (compound 2) was the only single amino acid substitution in WT-ImI with similar antagonist potency as the wild type peptide, as substitutions with Trp (compound 3) or Abu (compound 4) at this position yielded analogs with significantly lower antagonist potencies.

The analogs that displayed the most profound increases in antagonist potencies contained multiple substitutions of amino acids in the *n*-loop. The majority of the analogs containing Nva or Leu at O_9 displayed significantly increased antagonist potencies relative to WT-ImI. Furthermore, the most potent analogs containing Leu at O_9 also contained Abu at O_{11} (compounds 28, 32, and 36). However, most compounds containing Nva at O_9 displayed medium antagonist potency compared with Leu-containing analogs. Although it seems to be of little importance whether the O_{10}-position in the analogs was a Trp or a Tyr residue for their activities at the α_7 nAChR, analogs containing these two amino acids demonstrated increased antagonist potencies compared with analogs containing Phe in this position. Compounds 14, 16, 22, 28, 32, and 36 all demonstrated notably higher potency than WT-ImI, with compound 36 exhibiting 10 times more antagonist potency than the native α-conotoxin. Importantly, compound 14 (Nva^9–Trp^{10}–His^{11}), which was predicted to be the most active analog based on the initial PS-SCL screening data, was included in the group of analogs exhibiting high antagonist potency.

Structural Characterization of Selected ImI Analogs

Structural variations resulting from hypermutation of the ImI *n*-loop for a selection of the most potent analogs were

TABLE 2

Functional properties of the second series of individual α-conotoxin analogs at the α_7-GH3 cell line in the Fluo-4/Ca^{2+} assay

The assay was performed as described under "Experimental Procedures," and the data are the means of 3–5 individual experiments performed in duplicate. EC_{80}–EC_{90} concentrations of acetylcholine were used for the experiments. Fold differences were calculated as follows: (IC_{50} WT-ImI/IC_{50} analog)$^{-1}$ for analogs with increased antagonistic potency compared with WT-ImI (IC_{50} analog/IC_{50} WT-ImI)+1 for analogs with decreased antagonistic potency compared with WT-ImI. Examples of concentration-inhibitions curves for selected high antagonist potency analogs are shown in supplemental Fig. S1.

#	O_9	O_{10}	O_{11}	IC_{50} (μM)	$-\log_{10}[IC_{50}]$ ± S.E.M	Fold Difference	#	O_9	O_{10}	O_{11}	IC_{50} (μM)	$-\log_{10}[IC_{50}]$ ± S.E.M	Fold Difference
WT	Ala	Trp	Arg	4.4	5.35 ± 0.04	0	**19**	Nva	Phe	Trp	1.72	5.76 ± 0.04	1.56
2	Ala	Trp	His	2.64	5.58 ± 0.03	0.67	**20**	Nva	Phe	Abu	1.12	5.95 ± 0.04	2.93
3	Ala	Trp	Trp	17.1	4.77 ± 0.04	-2.89	**21**	Nva	Tyr	Arg	2.42	5.62 ± 0.03	0.82
4	Ala	Trp	Abu	27.0	4.57 ± 0.05	-5.14	**22**	Nva	Tyr	His	0.55	6.26 ± 0.04	7.00
5	Ala	Phe	Arg	~100	~4.0	-21.73	**23**	Nva	Tyr	Trp	1.05	5.98 ± 0.02	3.19
6	Ala	Phe	His	17.9	5.58 ± 0.03	-3.07	**24**	Nva	Tyr	Abu	0.75	6.12 ± 0.03	4.87
7	Ala	Phe	Trp	~31	4.51 ± 0.05	-6.05	**25**	Leu	Trp	Arg	2.54	5.60 ± 0.04	0.73
8	Ala	Phe	Abu	~100	~4.0	-21.73	**26**	Leu	Trp	His	1.20	5.92 ± 0.03	2.67
9	Ala	Tyr	Arg	27	4.56 ± 0.04	-5.14	**27**	Leu	Trp	Trp	0.84	6.08 ± 0.03	4.24
10	Ala	Tyr	His	2.67	5.57 ± 0.03	0.39	**28**	Leu	Trp	Abu	0.48	6.32 ± 0.04	8.17
11	Ala	Tyr	Trp	~100	~4.0	-21.73	**29**	Leu	Phe	Arg	1.69	5.77 ± 0.04	1.60
12	Ala	Tyr	Abu	~50	~4.3	-10.36	**30**	Leu	Phe	His	2.30	5.64 ± 0.03	0.91
13	Nva	Trp	Arg	13.0	4.88 ± 0.04	-1.95	**31**	Leu	Phe	Trp	2.15	5.67 ± 0.04	1.05
14	Nva	Trp	His	0.46	6.34 ± 0.04	8.57	**32**	Leu	Phe	Abu	0.64	6.19 ± 0.02	5.88
15	Nva	Trp	Trp	0.96	6.02 ± 0.03	3.58	**33**	Leu	Tyr	Arg	1.43	5.84 ± 0.04	2.08
16	Nva	Trp	Abu	0.51	6.29 ± 0.04	7.63	**34**	Leu	Tyr	His	1.00	6.00 ± 0.03	3.40
17	Nva	Phe	Arg	3.03	5.52 ± 0.03	0.45	**35**	Leu	Tyr	Trp	1.41	5.85 ± 0.05	2.12
18	Nva	Phe	His	0.94	6.03 ± 0.05	3.68	**36**	Leu	Tyr	Abu	0.44	6.36 ± 0.03	9.00

examined by NMR spectroscopy. NMR spectra were obtained for compounds 14, 16, 22, 24, 28, 32, and 36. NMR data were recorded at 285 K and showed single spin systems for each residue for all peptides. The spectra were assigned, and chemical shift analysis indicated that the Hα shift values of all peptides were comparable with those of the published values for WT-ImI (49), with only small local variations around the sites of mutation (Fig. 4*a*). Therefore, overall the chemical shifts of the analogs examined by NMR indicated the peptides were similar in structure to the globular isomer of WT-ImI.

The disulfide bond connectivity of compound 36 was unambiguously confirmed using a regioselective disulfide bond forming strategy. Both the globular and ribbon isomers were synthesized utilizing the orthogonal *S*-Acm and *S*-4-methylbenzyl combination in a two-step oxidation procedure. Co-injection of both isomers with the sample obtained from random oxidation confirmed its identity as the globular disulfide bond isomer.

The full three-dimensional structure of compound 36 was determined. Sufficient nuclear Overhauser effects were observed to calculate a three-dimensional structure using a simulated annealing protocol in CNS. A set of 50 structures was calculated with 51 distance restraints consisting of 38 sequential, 9 medium range, and 4 long range restraints. Eight ϕ angle restraints were included and 6 χ_1 angle restraints. The 20 lowest energy structures were chosen to represent the structure of compound 36, and structural statistics for this NMR ensemble are provided in supplemental Table 1, and the structural data have been deposited in the Biological Magnetic Resonance Bank. A well defined structure was obtained as shown by the root mean square deviation over residues 1–12 of 0.48 ± 0.28 Å for the backbone atoms and 0.99 ± 0.35 Å for heavy atoms. Analysis of the structures with PROMOTIF (36) identified a 3_{10} helix between residues 2 and 4, which is illustrated by the ribbon depiction in Fig. 4*b*, and a type I turn from residues 5 to 8.

A comparison of the structure of compound 36 with native ImI (Protein Data Bank code 1IM1) (51), shown in Fig. 4*c*, shows the high degree of similarity between the peptide backbones of the two molecules. The root mean square deviation of the backbone atoms of the mean structures from the two ensembles is only 0.82, although most of this difference is around the substituted residues in the *n*-loop. Furthermore, a comparison of the NMR solution structure of compound 36 with that of the known ImI/AChBP crystal structure showed that overall the backbone architecture is very similar with backbone root mean square deviation of only ~1 Å (18). The 21 conformations of NMR structure showed difference only in the dynamics of side chains of residues Arg^7 and Tyr^{10}.

Homology Modeling and Docking Studies

In an effort to further refine the activity and to gain additional insights into the binding interactions of the α-conotoxin ImI analogs with the α_7 nAChR, computational modeling and simulations were used for selected analogs. A homology model of the amino-terminal binding domain of α_7 nAChR was built using the AChBP/ImI x-ray crystal structure (Protein Data Bank code 2BYP) as a template (18). Two docking models were obtained using high and low antagonist potency analogs from the second iteration library. The pentameric nAChR structure was retained, superimposed from the template structure, and for each model the co-crystallized α-conotoxin was mutated according to the second iteration library α_7 nAChR functional assays. In Model 1, ImI was mutated to Leu^9–Trp^{10}–Abu^{11} (compound 28, high antagonist potency), and in Model 2 ImI was mutated to Ala^9–Phe^{10}–Arg^{11} (compound 5, inactive). Further refinement and analysis of both models were made on the basis of 500 ps of molecular dynamics simulations. Although a complete computation-based explanation of the structure-activity relationship studies of the 36 compounds in the second series of individual compounds is beyond the scope of this paper, the focused analysis on the final models of the three mutated residues revealed the following trends that were valuable in designing a third iteration library (Fig. 5).

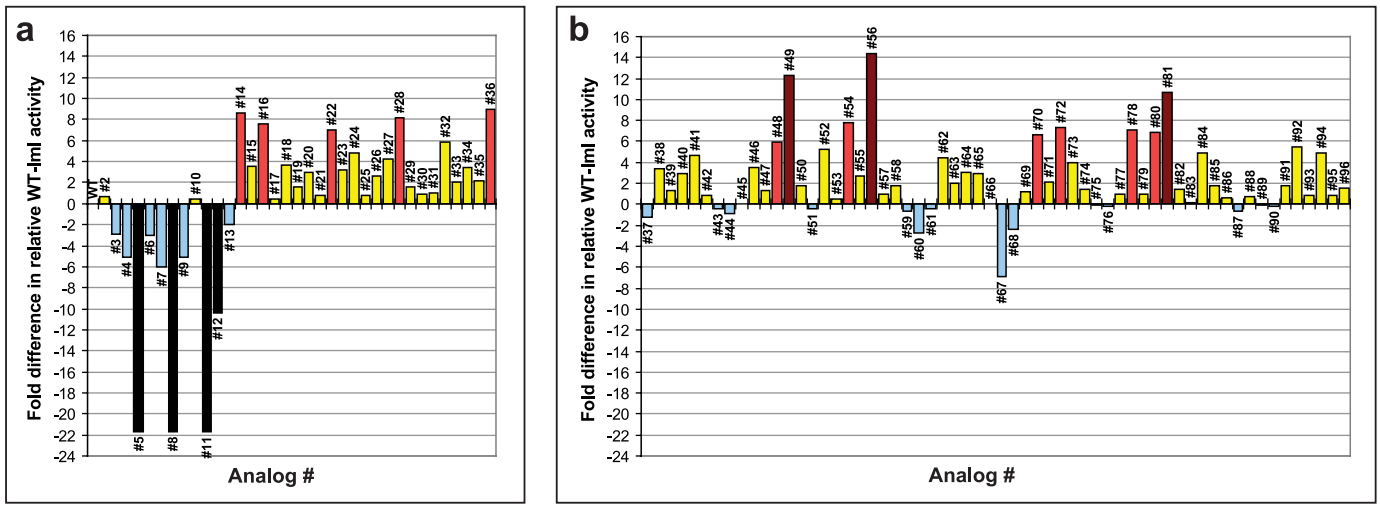

FIGURE 3. **Comparative potency of the second (*a*) and third (*b*) series of individual analogs at the α_7-GH3 cell line in the Ca^{2+}/Fluo-4 assay represented as relative fold differences in WT-Iml activities.** Each analog was tested as 3–5 individual experiments performed in duplicate. An assay concentration of 30 μM acetylcholine (EC_{80}–EC_{90}) was used for the experiments. *Dark red bars* are defined as very high potency analogs; *red*, high potency; *yellow*, medium potency; *cyan*, low potency; and *black*, inactive.

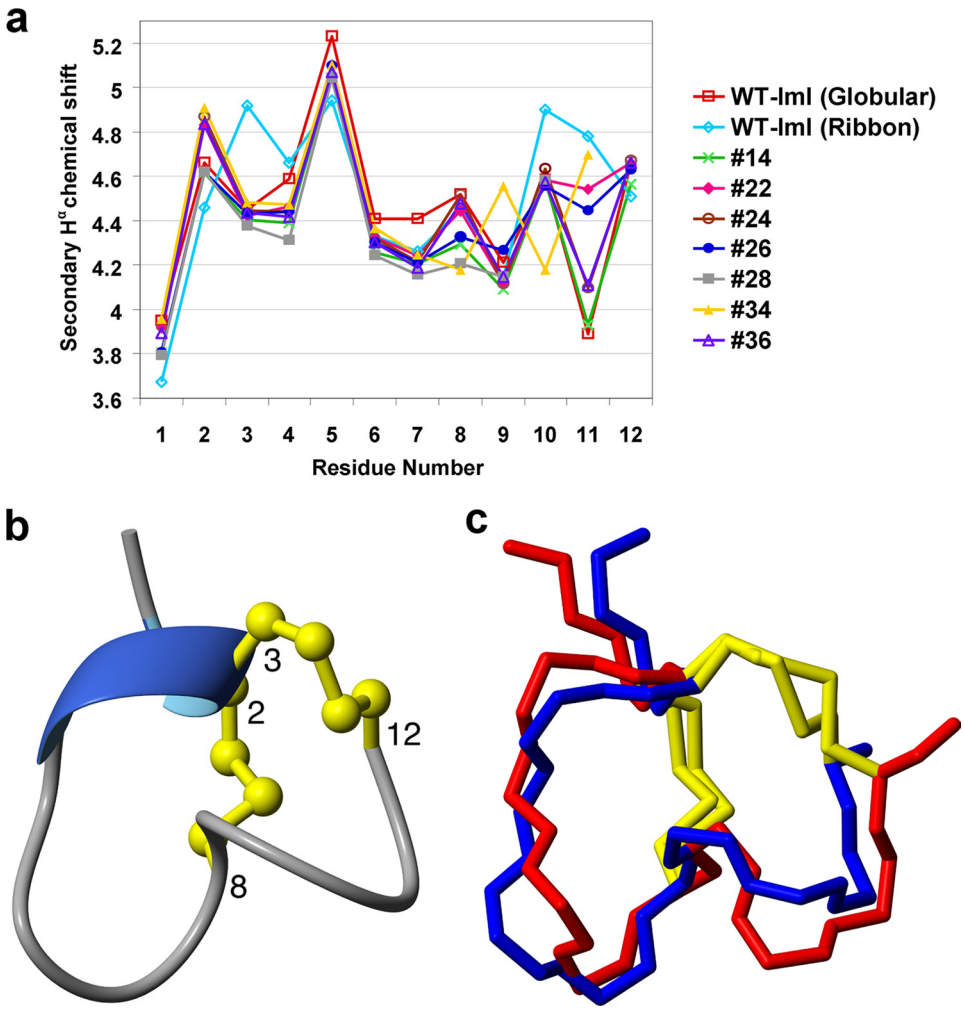

FIGURE 4. **NMR solution structure of analog 36.** *a*, secondary H^{α} chemical shifts. *b*, *ribbon representation* with disulfide bonds shown in *yellow*. *c*, overlay of the structures of WT-Iml (*red*) and compound 36 (*blue*).

O^9-position (Fig. 5a)—The Leu^9 residue in compound 28 was observed to participate in minor hydrophobic interactions with the α_7 receptor, but overall, the residue was in a pocket lined with the following hydrophobic residues: Leu^{118}(A) and Trp^{54}(A) on one side and Met^{159}(A) and Ser^{33}(A) on the other. Two polar residues, Gln^{56}(A) and Gln^{116}(A), also contributed to this pocket. All of these residues were part of only one subunit (shown as subunit A with residues in the text and in *cyan* in Fig. 5*a*) of the α_7 nAChR. Given the size of this pocket, it was only partially occupied by Leu^9 from the α-conotoxin. From these analyses, we hypothesized that mutations at this position for residues that are either too small and/or with less hydrophobic side chain will further reduce the hydrophobic contacts thus resulting in a loss of affinity/antagonist potency.

O^{10}-position (Fig. 5b)—This residue is situated in an outside pocket that upon visual inspection appears amenable for accommodating aromatic residues. Aromatic substitutions display cation-π interaction with Arg^{78}(A) in some of the conformations during the Molecular Dynamics simulation. Overall, the receptor residues surrounding this residue originated from both the subunits of nAChR, as shown in *cyan* and *magenta* in Fig. 5*b*.

O^{11}-position (Fig. 5c)—This residue is outside the binding pocket and appears not to participate in any major interactions during the simulation of complex with compound 28.

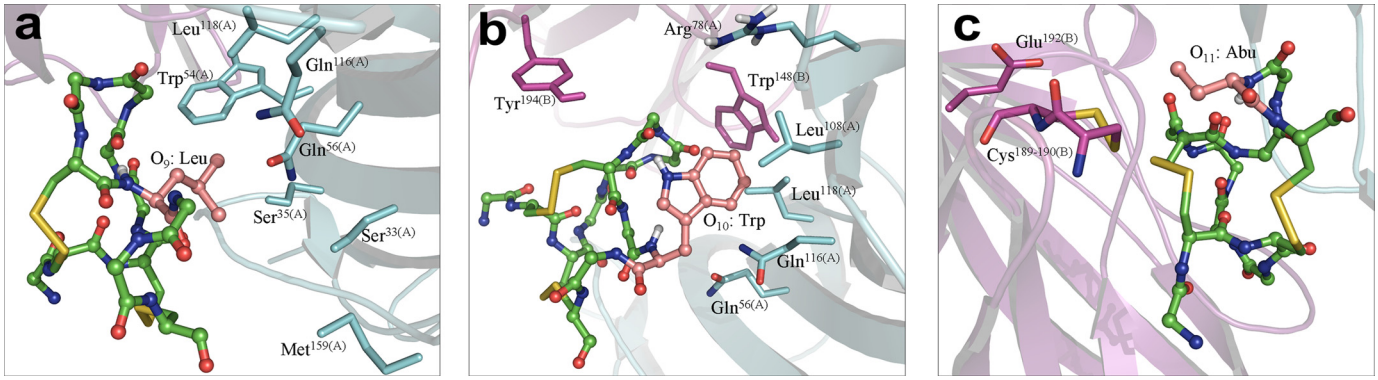

FIGURE 5. **Binding model of compound 28 into the binding pocket of a homology model of α_7 nAChR.** The binding sub-pockets of the three mutated residues of the α-conotoxin are shown, *a*, O_9; *b*, O_{10}; and *c*, O_{11}. In all the structures, conotoxin is shown as *ball and stick model* of backbone atoms (*green carbon*) with side chain of each mutated residue (*pink carbon*). Receptor is shown in slightly transparent cartoon model (colored by chain *magenta* and *cyan*). The binding site residues are shown only as *stick models* (carbon color colored by chain). Only polar hydrogen atoms are shown.

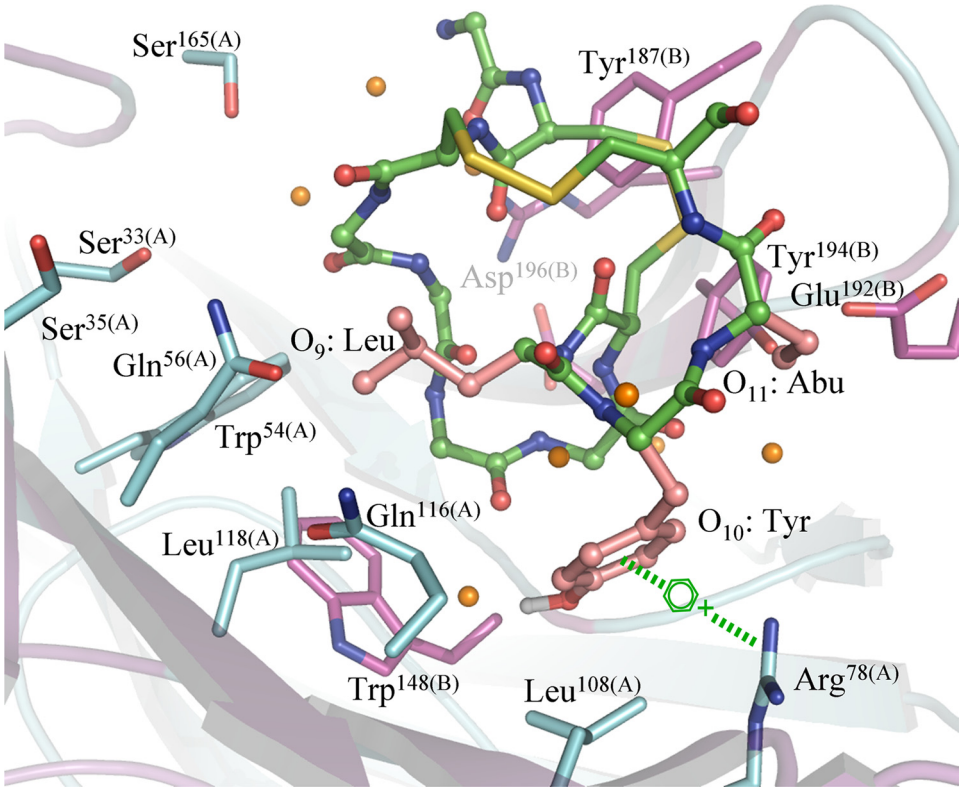

FIGURE 6. **Binding model of compound 36 into the binding pocket of a homology model of α_7 nAChR.** The binding site view of the two α_7 nAChR subunits with docked and optimized α-conotoxin (compound 36) is shown. The α-conotoxin is shown as *ball and stick model* of backbone atoms (*green carbon*) with side chains shown only for three mutated *n*-loop residues (*pink carbon*). Receptor is shown in slightly transparent *cartoon* model (colored by chain *cyan* (*A*) and *magenta* (*B*)). The binding site residues are shown only as *stick models* (carbon color colored by chain). Water molecules are shown as *orange spheres*, and only polar hydrogen atoms of side chains are shown.

The structure of compound 36, obtained from NMR analysis, was also modeled into the binding site of homology model of the α_7 receptor (Fig. 6). The analysis of this complex identified several amino acid residues from the receptor that contribute to the α-conotoxin-binding site. As established previously from the known crystal and modeled structures, the binding site of the α-conotoxin is surrounded by charged aromatic and hydrophobic residues. Notably, as shown in Fig. 6, these residues are as follows: acidic, Asp^{163}(A), Glu^{192}(B), and Asp^{196}(B); basic, Arg^{78}(A) and Arg^{185}(B); aromatic, Trp^{54}(A), Tyr^{92}(B), Trp^{148}(B), Tyr^{150}(B), Tyr^{187}(B), and Tyr^{194}(B); hydrophobic, Leu^{108}(A), Leu^{118}(A), and Pro^{195}(B); and polar, Gln^{56}(A), Ser^{35}(A), Ser^{165}(A), Cys^{189}(B), Cys^{190}(B), Ser^{147}(B), and Ser^{149}(B). (Note: Some of the residues, Asp^{163}(A), Tyr^{92}(B), Tyr^{150}(B), Pro^{195}(B), Cys^{189}(B), Cys^{190}(B), Ser^{147}(B), and Ser^{149}(B), are shown only in the Molecular Operating Environment interaction map supplied as supplemental Fig. S2).

Three main direct interactions were observed in the optimized model. Two hydrogen bonds are between Arg^7 and Ser^4 of compound 36 and Asp^{196}(B) and Ser^{35}(A) of receptor, respectively, and one cation-π interaction is between Tyr^{10} of compound 36 and Arg^{78}(A) of receptor. The distance between the electron-rich π-ring of Tyr^{10} and the charged guanidine group of Arg^{78}(A) was ~4 Å.

Water molecules modeled from the crystal structure of AChBP, and optimized along with docked compound 36, appear to play an important role in the binding. These water molecules primarily act as direct or indirect mediators between the binding site residues and compound 36. These interactions cannot be seen in Fig. 6, where only the mutated residues of the α-conotoxin are shown (the various interactions of these water molecules are shown in the Molecular Operating Environment interaction map in supplemental Fig. S2).

Functional Characterization of a Third Iteration Library of Individual Compounds

In an effort to further refine the α_7 nAChR activities of the most potent α-conotoxin ImI analogs from the second series library, a third series of individual compounds was generated.

TABLE 3

Functional properties of the third series of individual α-conotoxin analogs at the α_7-GH3 cell line in the Fluo-4/Ca^{2+} assay

The assay was performed as described under "Experimental Procedures," and the data are the means of 3–5 individual experiments performed in duplicate. EC_{80}–EC_{90} concentrations of acetylcholine were used for the experiments. Fold differences were calculated as described in Table 2. Examples of concentration-inhibition curves for selected high and very high antagonist potency analogs are shown in supplemental Fig. S1.

#	O_9	O_{10}	O_{11}	IC_{50} (μM)	$-\log_{10}[IC_{50}]$ ± S.E.M	Fold Difference	#	O_9	O_{10}	O_{11}	IC_{50} (μM)	$-\log_{10}[IC_{50}]$ ± S.E.M	Fold Difference
WT	Ala	Trp	Arg	2.92	5.53 ± 0.05	0							
37	Leu	Nph	His	6.34	5.20 ± 0.05	-1.17	**67**	Nva	Cha	Abu	23	4.63 ± 0.07	-6.88
38	Leu	Nal	His	0.67	6.17 ± 0.04	3.36	**68**	Nva	Ile	Abu	15	4.82 ± 0.05	-2.41
39	Leu	Mty	His	1.26	5.90 ± 0.04	1.32	**69**	Leu	Nph	Trp	1.30	5.89 ± 0.03	1.25
40	Leu	Aph	His	0.74	6.13 ± 0.04	2.95	**70**	Leu	Nal	Trp	0.38	6.42 ± 0.05	6.68
41	Leu	Dmt	His	0.52	6.28 ± 0.05	4.62	**71**	Leu	Mty	Trp	0.93	6.03 ± 0.06	2.14
42	Leu	Pyr	His	1.56	5.81 ± 0.04	0.87	**72**	Leu	Aph	Trp	0.35	6.46 ± 0.05	7.34
43	Leu	Cha	His	6.30	5.20 ± 0.05	-0.43	**73**	Leu	Dmt	Trp	0.58	6.27 ± 0.07	4.03
44	Leu	Ile	His	3.70	5.43 ± 0.05	-0.84	**74**	Leu	Pyr	Trp	1.18	5.93 ± 0.03	1.47
45	Nva	Nph	His	2.79	5.55 ± 0.04	0.05	**75**	Leu	Cha	Trp	3.09	5.51 ± 0.05	-0.06
46	Nva	Nal	His	0.64	6.19 ± 0.03	3.56	**76**	Leu	Ile	Trp	3.39	5.47 ± 0.05	-0.16
47	Nva	Mty	His	1.24	5.91 ± 0.05	1.35	**77**	Nva	Nph	Trp	1.49	5.83 ± 0.06	0.96
48	Nva	Aph	His	0.42	6.38 ± 0.05	5.95	**78**	Nva	Nal	Trp	0.36	6.44 ± 0.04	7.11
49	Nva	Dmt	His	0.22	6.66 ± 0.03	12.27	**79**	Nva	Mty	Trp	1.44	5.84 ± 0.05	1.03
50	Nva	Pyr	His	1.06	5.97 ± 0.04	1.75	**80**	Nva	Aph	Trp	0.37	6.43 ± 0.05	6.89
51	Nva	Cha	His	4.23	5.37 ± 0.02	-0.45	**81**	Nva	Dmt	Trp	0.25	6.60 ± 0.04	10.68
52	Nva	Ile	His	0.47	6.33 ± 0.04	5.21	**82**	Nva	Pyr	Trp	1.22	5.91 ± 0.05	1.39
53	Leu	Nph	Abu	1.90	5.72 ± 0.05	0.54	**83**	Nva	Cha	Trp	2.43	5.61 ± 0.06	0.20
54	Leu	Nal	Abu	0.33	6.48 ± 0.06	7.85	**84**	Nva	Ile	Trp	0.49	6.31 ± 0.05	4.96
55	Leu	Mty	Abu	0.78	6.11 ± 0.04	2.74	**85**	Ile	Tyr	His	1.06	5.97 ± 0.04	1.75
56	Leu	Aph	Abu	0.19	6.72 ± 0.03	14.37	**86**	Val	Tyr	His	1.83	5.74 ± 0.05	0.60
57	Leu	Dmt	Abu	1.51	5.82 ± 0.06	0.93	**87**	Cha	Tyr	His	4.91	5.31 ± 0.04	-0.68
58	Leu	Pyr	Abu	1.06	5.97 ± 0.05	1.75	**88**	Nle	Tyr	His	1.70	5.77 ± 0.06	0.72
59	Leu	Cha	Abu	4.71	4.71 ± 0.03	-0.61	**89**	Phe	Tyr	His	3.20	5.49 ± 0.03	-0.09
60	Leu	Ile	Abu	11	5.97 ± 0.05	-2.77	**90**	Nal	Tyr	His	3.33	5.48 ± 0.06	-0.14
61	Nva	Nph	Abu	3.98	5.40 ± 0.07	-0.36	**91**	Ile	Trp	His	1.07	5.97 ± 0.04	1.73
62	Nva	Nal	Abu	0.54	6.27 ± 0.04	4.41	**92**	Val	Trp	His	0.45	6.34 ± 0.03	5.49
63	Nva	Mty	Abu	0.97	6.01 ± 0.04	2.01	**93**	Cha	Trp	His	1.61	5.79 ± 0.05	0.81
64	Nva	Aph	Abu	0.73	6.14 ± 0.06	3.00	**94**	Nle	Trp	His	0.49	6.31 ± 0.04	4.96
65	Nva	Dmt	Abu	0.75	6.12 ± 0.04	2.89	**95**	Phe	Trp	His	1.58	5.80 ± 0.03	0.85
66	Nva	Pyr	Abu	2.75	5.56 ± 0.05	0.06	**96**	Nal	Trp	His	1.17	5.93 ± 0.04	1.50

Two sub-libraries were synthesized to probe the O_9- and O_{10}-positions, respectively, based on docking studies of selected analogs into the α_7 nAChR homology model and functional data for second series library analogs at the α_7 nAChR. The first sub-library consisted of a series of analogs probing the O_{10}-position and incorporated six non-natural aromatic amino acids, including 4-nitrophenylalanine (Nph), napth-1-ylalanine (Nal), *O*-methyltyrosine (Mty), 4-aminophenylalanine (Aph), 2,6-dimethyltyrosine (Dmt), 3-pyridinylalanine (Pyr), as well the nonaromatic hydrophobic amino acids Ile and cyclohexylalanine (Cha). These were used in combination with Leu or Nva residues in the O_9-position, and His, Abu, or Trp residues in the O_{11}-position to give a total of 48 individual analogs. The second sub-library probed the O_9-position with a series of hydrophobic amino acids including Ile, Val, Cha, Nle, Phe, and Nal residues in combination with Tyr or Trp in the O_{10}-position and a residue His in the O_{11}-position to give 12 additional analogs. In total, 60 additional individual analogs were synthesized in the third iteration library, and their antagonist potencies were determined at the α_7 nAChR in the Fluo-4/Ca^{2+} assay (Table 3 and Fig. 3*b*).

Although a majority of the analogs in the O_9 sub-library displayed medium antagonist potencies, none of these compounds surpassed corresponding analogs containing Nva or Leu at this position. However, profound increases in antagonistic potency were observed for several analogs in the O_{10} sub-library. Compounds 49 (Nva^9–Dmt^{10}–His^{11}), 56 (Leu^9–Aph^{10}–Abu^{11}), and 81 (Nva^9–Dmt^{10}–Trp^{11}) all exhibited very high antagonist potencies, with the most active analog, compound 56, exhibiting a more than 14-fold increase compared with WT-ImI. Furthermore, there is trend in antagonistic potency of analogs bearing a strongly activating substituent on the aromatic ring, with several analogs containing Tyr-, Dmt- and Aph- in the O_{10}-position exhibiting high or very high antagonist potency. On the other hand, analogs containing Mty, Nph, or Pyr in the O_{10}-position all exhibited similar antagonist potencies to WT-ImI. Analogs containing Nal in the O_{10}-position displayed significantly increased antagonist potencies across all samples and displayed comparable antagonist potency to corresponding analogs containing Trp. On the other hand, the nonaromatic amino acid Cha and Ile O_{10} analogs generally exhibited lower antagonistic potencies. Five of six compounds with Cha at O_{10} (compounds 43, 51, 59, 67, and 75) showed low antagonist potency. In general, these observations are in agreement with the trend derived in the modeling where it was concluded that an aromatic residue at O_{10} is beneficial for the activity.

The pairwise structure-activity relationships for both the second and third iteration libraries of individual analogs were examined to determine the optimal combinations of amino

acid functionalities for the synthesized analogs (Fig. 7). For the O_9–O_{10} combination (Fig. 7*a*), the Nva^9-Dmt^{10} combination led to two of the three very high antagonist potency analogs. Similarly, the Leu^9–Aph^{10}, Nva^9–Aph^{10}, and Leu^9–Nal^{10} combinations lead the same numbers of analogs displaying high to very high antagonist potencies. Other combinations for O_9–O_{10} that yielded high antagonist potency include Nva^9–Trp^{10}, Nva^9–Tyr^{10}, Leu^9–Trp^{10}, and Leu^9–Tyr^{10}. For the O_9–O_{11} combination (Fig. 7*b*), all Nva^9–Trp^{11} analogs displayed increased antagonist potency compared with WT-ImI, with four compounds exhibiting high or very high potency and 11 displaying medium antagonist potencies. The Nva^9–His^{11} and Leu^9–Abu^{11} combinations also yielded four compounds with high or very high potency, with one and two low antagonist potency analogs, respectively. For the O_{10}–O_{11} combination (Fig. 7*c*), Aph^{10}–Abu^{11}, Dmt^{10}–His^{11}, and Dmt^{10}–Trp^{11} containing analogs each yielded one compound with very high and one compound with medium antagonist potency. Analogs containing the Aph^{10}–Trp^{11}, Nal^{10}–Trp^{11}, and Trp^{10}–Abu^{11} combinations each yielded two high antagonist potency analogs. The most dramatic change in activity is observed for the analogs containing Tyr^{10}–Abu^{11} (Fig. 7*c*) that yield one compound with high antagonist potency (compound 36, Leu^9; IC_{50} = 0.44 μM) and one compound regarded as inactive (compound 12, Ala^9; IC_{50} ~ 50 μM).

Further Functional Characterization of Selected ImI Analogs—The high and very high antagonist potency analogs identified in the second and third iteration libraries were screened for activities at $\alpha_4\beta_2$ and $\alpha_3\beta_4$ nAChR subtypes to assess their selectivity for the α_7 nAChR toward these two other major neuronal nAChR subtypes. This was achieved using cell lines stably expressing the rat $\alpha_3\beta_4$ nAChR and the mouse $\alpha_4\beta_2$ nAChR using the Fluo-4/Ca^{2+} assay and the fluorescent imaging plate reader membrane potential blue assay, respectively (39, 40). No significant antagonist activity was observed for any of these analogs at these two subtypes at concentrations up to 300 μM, except for analog 81, which only displayed moderate inhibition (~50%) at a concentration of 300 μM (supplemental Table S2). This indicates that all very high and high antagonist potency ImI analogs are characterized by high degrees of selectivity for the α_7 nAChR over $\alpha_4\beta_2$ and $\alpha_3\beta_4$.

DISCUSSION

To date, a majority of structure-activity relationship studies on α-conotoxins as nAChR ligands have largely focused on single amino acid substitutions to study the roles of specific positions within the *m*- and *n*-loop regions (8–16). In this study, we have utilized a three-step synthetic combinatorial strategy to study a specific region (*i.e.* the *n*-loop) of α-conotoxin ImI to develop novel analogs with improved antagonist properties for the α_7 nAChR.

Synthesis of Mixture-based α-Conotoxin Libraries—Although other methods have previously been reported for the high throughput synthesis of conopeptides (52, 53), our approach has involved parallel Boc-SPPS using tea bags, two-step low-high HF cleavage with a multiple cleavage manifold and oxidative formation of disulfide bonds. To our knowledge, this is the first study that has applied synthetic mixture-based

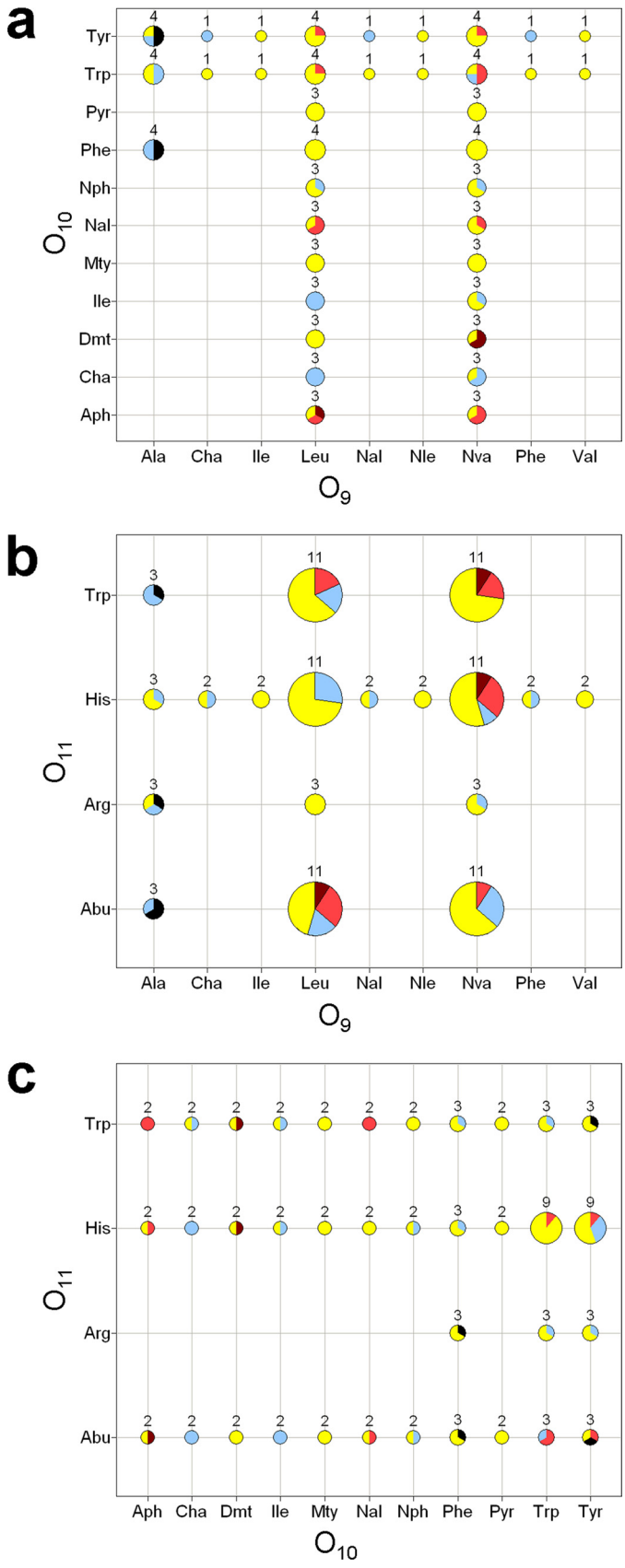

FIGURE 7. **Pairwise structure-activity relationships for amino acids in the O_9–O_{10} (*a*), O_9–O_{11} (*b*), and O_{10}-O_{11}-positions (*c*).** The relative size of each *pie graph* is proportional to the number of analogs synthesized and screened. *Dark red*, very high; *red*, high; *yellow*, medium; *cyan*, low; *black*, inactive antagonist potency at the α_7 nAChR.

combinatorial libraries specifically to conotoxins, which has proven to be a time- and cost-effective approach to generating large amounts of information regarding specific residues in a conotoxin sequence.

It is known that mature conotoxin sequences contain all the necessary information to achieve correct *in vitro* oxidative folding (54). Even though our synthetic approach utilized oxidation conditions optimized for the synthesis of WT-ImI, individual analogs were often accompanied by the presence of other non-native disulfide bond isomers. Moreover, the formation of disulfide bond isomers in PS-SCL mixtures cannot be determined directly. As such, misfolded conotoxins would be expected to be present in the PS-SCL mixtures. Given that correct conotoxin folding is sequence-driven, misfolded analogs would be expected to be inactive and would not contribute to any activity in the initial PS-SCL screening assay. However, the non-native ribbon isomer of α-conotoxin AuIB displays a 10-fold increased activity at the $\alpha_3\beta_4$ nAChR compared with the native α-conotoxin (50). In this regard, highly active misfolded isomers in mixtures would be expected to increase the level of diversity of conotoxin PS-SCLs. These can be identified when they are individually synthesized.

Structure-Activity Relationships of the α-Conotoxin ImI Analogs at the α_7 nAChR—Through screening and deconvolution of a PS-SCL via a fluorescence-based functional assay at the α_7 nAChR, specific amino acid residue substitutions in the *n*-loop were identified as promising candidates for the development of more potent α-conotoxin ImI analog antagonists.

Of the total 96 individual analogs synthesized in this study, three analogs were found to exhibit very high potency, 11 high potency, 58 medium potency, and 20 low potency, and four analogs were found to be inactive as α_7 nAChR antagonists. Furthermore, a selection of the most potent α_7 nAChR antagonists identified in this series was found to be highly selective for this subtype over the $\alpha_3\beta_4$ and $\alpha_4\beta_2$ subtypes. The most significant increases in antagonist potency were observed for analogs containing the Nva^9–Dmt^{10}–His^{11}, Leu^9–Aph^{10}–Abu^{11}, and Nva^9–Dmt^{10}–Trp^{11} combinations (compounds 49, 56, and 81), which exhibited ~12-, 14-, and 10-fold increases, respectively, when compared with WT-ImI. To our knowledge, these compounds represent the most potent α-conotoxin ImI analogs reported to date.

One of the most notable observations arising from this study is the complexity of the contribution of the *n*-loop of α-conotoxin ImI to its binding to α_7 nAChR, where no single substitution resulted in increased antagonist potency. Rather, substitutions acted synergistically to achieve significant increases in antagonist potency, underlining the efficacy of our combinatorial approach at multiple positions. Although this suggests that the functionalities of the *n*-loop residues in native toxin are quite optimized for its interactions with the receptors, the antagonist activity of it *can* be significantly enhanced by combinations of two or three residue substitutions in the loop.

Substitutions of Ala with Nva or Leu residues in the O_9-position of the peptide were found to be optimal for α_7 nAChR activity in the PS-SCL mixtures. This constituted the rationale for the focus on these residues as O_9 substitutions in the individual analogs in the second and third iteration libraries. Molecular modeling of selected compounds from the second iteration library revealed that small amino acids such as Ala at O_9 might lack sufficient hydrophobic interactions within the binding sub-pocket. Actually, only Nva stood out in the PS-SCL analysis, as the functional data for the Leu^9 analog mixture did not differ significantly from many other PS-SCL O_9 mixtures (Table 1). The superiority of Nva over Leu in this position translated from the PS-SCL into the individually synthesized analogs.

The presence of an aromatic residue in the O_{10}-position of α-conotoxin ImI, as in the case of the native Trp, was observed to be crucial for optimal receptor binding. This observation is supported by the fact that analogs containing Cha and Ile in the O_{10}-position typically display lower antagonist potencies than their corresponding Trp, Nph, Nal, Mty, Aph, Dmt, and Pyr analogs. Deviations from this general trend do exist in the series, however, as the Ile^{10}-containing analogs 52 and 84 are quite potent as α_7 antagonists (Table 3).

Another observation regarding the O_{10} residue is that large aromatic side chain functionalities such as the native Trp and Nal in this position generally increase the antagonistic potency of the analogs. This observation might be associated with cation-π interaction between the aromatic residue at O_{10} and Arg^{78}(A) in the binding site. Significantly, analogs with aromatic residues bearing strongly activating moieties that increase electron density into the aromatic ring (*i.e.* Tyr, –OH; Dmt, –OH, and $-CH_3$; and Aph, $-NH_2$ substituents) in the O^{10}-position also yield considerable increases in antagonistic potency, indicating stronger cation-π interactions with Arg^{78}(A) in the receptor-binding site. As such, each of the very high antagonist potency analogs (compounds 49, 56, and 81) possessed either Dmt or Aph at position O_{10}. Conversely, Mty, Nph, and Pyr containing analogs each exhibited no significant difference in antagonistic potency, which is possibly a result of a deactivated aromatic ring that weakens the interaction with Arg^{78}(A).

In general, substitutions in the O_{11}-position in the *n*-loop had minor effects on antagonistic potency. Furthermore, it can be confirmed by comparisons of the IC_{50} values of the various groups of three analogs containing the same residues in the O_9- and O_{10}-positions and having Trp, His, or Abu residues in the O_{11}-position. Finally, Abu, His, and Trp as O_{11} residues were all found in the four very high antagonist potency analogs. This can be explained in terms of the O_{11}-position being oriented away from the binding site and not taking part in any significant interactions with the receptor *per se*. Thus, the functional data of the analogs are in agreement with the observations from the molecular modeling. However, it should be stressed that the O_{11}-position was not probed to the same extent in the third series of compounds as the O_9- and O_{10}-positions.

One of the most striking outcomes from this study is that the most potent individual compound predicted from the screening data (Nva^9–Trp^{10}–His^{11}, compound 14) was among the most potent analogs in the second series of compounds. This result underlines the efficacy of PS-SCL mixtures for identifying analogs with amino acid combinations giving rise to improved functional activities for a given pharmacological target.

Additional probing of other regions of α-conotoxin ImI could also lead to higher potency antagonists. For example, we recently reported that substitution of Pro^6 with 5-(*R*)-phenylproline in α-conotoxin ImI induces π-stacking interactions with another underutilized binding pocket (14). As such, we speculate that substituting Pro^6 with 5-(*R*)-phenylproline in the very high potency antagonists arising from this study would result in even greater increases in antagonistic potency at the α_7 nAChR.

Future Perspectives—Given the importance of the α_7 nAChR in memory, cognition, and in overall mental health (5, 6), the development of potent and selective ligands for this receptor would be of major significance for researchers studying its role in neuropathological conditions such as schizophrenia, Alzheimer, and Parkinson disease. Although this study has focused on the development of α-conotoxin ImI analogs with increased antagonist activity and subtype selectivity at the α_7 nAChR, it is expected that screening of the α-conotoxin ImI *n*-loop PS-SCL for activity at the $\alpha_9\alpha_{10}$ nAChR will identify a different set of active amino acid functionalities, allowing the design of individual analogs with enhanced activities for this receptor. Finally, the construction of PS-SCLs based on other classes of conotoxins seems to be a promising strategy to develop new subtype-selective ligands targeting other nAChR subtypes, just as other disulfide-rich venom peptides could be used as scaffolds in PS-SCL-based design for other therapeutically relevant targets.

Acknowledgments—We gratefully acknowledge the generous gifts of the cell lines stably expressing the human α_7, the mouse $\alpha_4\beta_2$, and the rat $\alpha_3\beta_4$ nAChRs from Dr. Dominik Feuerbach (Novartis Institute of Biomedical Research, Basel, Switzerland), Dr. Jerry A. Stitzel (University of Colorado, Boulder), and Drs. Ken Kellar and Yingxian Xiao (Georgetown University School of Medicine, Washington, D. C.), respectively. We thank Drs. Clemencia Pinilla, Adel Nefzi, and Marc Giulianotti for valuable discussions.

REFERENCES

1. Armishaw, C. J., and Alewood, P. F. (2005) *Curr. Protein Pept. Sci.* **6,** 221–240
2. Sollod, B. L., Wilson, D., Zhaxybayeva, O., Gogarten, J. P., Drinkwater, R., and King, G. F. (2005) *Peptides* **26,** 131–139
3. Han, T. S., Teichert, R. W., Olivera, B. M., and Bulaj, G. (2008) *Curr. Pharm. Des.* **14,** 2462–2479
4. Dani, J. A., and Bertrand, D. (2007) *Annu. Rev. Pharmacol. Toxicol.* **47,** 699–729
5. Taly, A., Corringer, P. J., Guedin, D., Lestage, P., and Changeux, J. P. (2009) *Nat. Rev. Drug Discov.* **8,** 733–750
6. Jensen, A. A., Frølund, B., Liljefors, T., and Krogsgaard-Larsen, P. (2005) *J. Med. Chem.* **48,** 4705–4745
7. Azam, L., and McIntosh, J. M. (2009) *Acta Pharmacol. Sin.* **30,** 771–783
8. Quiram, P. A., and Sine, S. M. (1998) *J. Biol. Chem.* **273,** 11007–11011
9. Utkin, Y. N., Zhmak, M. N., Methfessel, C., and Tsetlin, V. I. (1999) *Toxicon* **37,** 1683–1695
10. Rogers, J. P., Luginbühl, P., Pemberton, K., Harty, P., Wemmer, D. E., and Stevens, R. C. (2000) *J. Mol. Biol.* **304,** 911–926
11. Hogg, R. C., Hopping, G., Alewood, P. F., Adams, D. J., and Bertrand, D. (2003) *J. Biol. Chem.* **278,** 26908–26914
12. Kasheverov, I. E., Zhmak, M. N., Vulfius, C. A., Gorbacheva, E. V., Mordvintsev, D. Y., Utkin, Y. N., van Elk, R., Smit, A. B., and Tsetlin, V. I. (2006) *FEBS J.* **273,** 4470–4481
13. Azam, L., Yoshikami, D., and McIntosh, J. M. (2008) *J. Biol. Chem.* **283,** 11625–11632
14. Armishaw, C., Jensen, A. A., Balle, T., Clark, R. J., Harpsøe, K., Skonberg, C., Liljefors, T., and Strømgaard, K. (2009) *J. Biol. Chem.* **284,** 9498–9512
15. Millard, E. L., Nevin, S. T., Loughnan, M. L., Nicke, A., Clark, R. J., Alewood, P. F., Lewis, R. J., Adams, D. J., Craik, D. J., and Daly, N. L. (2009) *J. Biol. Chem.* **284,** 4944–4951
16. Halai, R., Clark, R. J., Nevin, S. T., Jensen, J. E., Adams, D. J., and Craik, D. J. (2009) *J. Biol. Chem.* **284,** 20275–20284
17. Celie, P. H., Kasheverov, I. E., Mordvintsev, D. Y., Hogg, R. C., van Nierop, P., van Elk, R., van Rossum-Fikkert, S. E., Zhmak, M. N., Bertrand, D., Tsetlin, V., Sixma, T. K., and Smit, A. B. (2005) *Nat. Struct. Mol. Biol.* **12,** 582–588
18. Hansen, S. B., Sulzenbacher, G., Huxford, T., Marchot, P., Taylor, P., and Bourne, Y. (2005) *EMBO J.* **24,** 3635–3646
19. Ulens, C., Hogg, R. C., Celie, P. H., Bertrand, D., Tsetlin, V., Smit, A. B., and Sixma, T. K. (2006) *Proc. Natl. Acad. Sci. U.S.A.* **103,** 3615–3620
20. Dutertre, S., Ulens, C., Büttner, R., Fish, A., van Elk, R., Kendel, Y., Hopping, G., Alewood, P. F., Schroeder, C., Nicke, A., Smit, A. B., Sixma, T. K., and Lewis, R. J. (2007) *EMBO J.* **26,** 3858–3867
21. Ellison, M., and Olivera, B. M. (2007) *Chem. Rec.* **7,** 341–353
22. Franco, A., Pisarewicz, K., Moller, C., Mora, D., Fields, G. B., and Marì, F. (2006) *Prog. Mol. Subcell. Biol.* **43,** 83–103
23. Pinilla, C., Appel, J. R., Blanc, P., and Houghten, R. A. (1992) *BioTechniques* **13,** 901–905
24. Dooley, C. T., and Houghten, R. A. (1993) *Life Sci.* **52,** 1509–1517
25. Houghten, R. A., Pinilla, C., Appel, J. R., Blondelle, S. E., Dooley, C. T., Eichler, J., Nefzi, A., and Ostresh, J. M. (1999) *J. Med. Chem.* **42,** 3743–3778
26. Dooley, C. T., Ny, P., Bidlack, J. M., and Houghten, R. A. (1998) *J. Biol. Chem.* **273,** 18848–18856
27. Pinilla, C., Rubio-Godoy, V., Dutoit, V., Guillaume, P., Simon, R., Zhao, Y., Houghten, R. A., Cerottini, J. C., Romero, P., and Valmori, D. (2001) *Cancer Res.* **61,** 5153–5160
28. Nino-Vasquez, J. J., Allicotti, G., Borras, E., Wilson, D. B., Valmori, D., Simon, R., Martin, R., and Pinilla, C. (2004) *Mol. Immunol.* **40,** 1063–1074
29. Houghten, R. A. (1985) *Proc. Natl. Acad. Sci. U.S.A.* **82,** 5131–5135
30. Schnölzer, M., Alewood, P., Jones, A., Alewood, D., and Kent, S. B. (1992) *Int. J. Pept. Protein Res.* **40,** 180–193
31. Ostresh, J. M., Winkle, J. H., Hamashin, V. T., and Houghten, R. A. (1994) *Biopolymers* **34,** 1681–1689
32. Güntert, P., Mumenthaler, C., and Wüthrich, K. (1997) *J. Mol. Biol.* **273,** 283–298
33. Brünger, A. T., Adams, P. D., Clore, G. M., DeLano, W. L., Gros, P., Grosse-Kunstleve, R. W., Jiang, J. S., Kuszewski, J., Nilges, M., Pannu, N. S., Read, R. J., Rice, L. M., Simonson, T., and Warren, G. L. (1998) *Acta Crystallogr. D Biol. Crystallogr.* **54,** 905–921
34. Clark, R. J., Fischer, H., Nevin, S. T., Adams, D. J., and Craik, D. J. (2006) *J. Biol. Chem.* **281,** 23254–23263
35. Koradi, R., Billeter, M., and Wüthrich, K. (1996) *J. Mol. Graph.* **14,** 51–55
36. Hutchinson, E. G., and Thornton, J. M. (1996) *Protein Sci.* **5,** 212–220
37. Laskowski, R. A., Rullmannn, J. A., MacArthur, M. W., Kaptein, R., and Thornton, J. M. (1996) *J. Biomol. NMR* **8,** 477–486
38. Feuerbach, D., Lingenhöhl, K., Dobbins, P., Mosbacher, J., Corbett, N., Nozulak, J., and Hoyer, D. (2005) *Neuropharmacology* **48,** 215–227
39. Xiao, Y., Meyer, E. L., Thompson, J. M., Surin, A., Wroblewski, J., and Kellar, K. J. (1998) *Mol. Pharmacol.* **54,** 322–333
40. Karadsheh, M. S., Shah, M. S., Tang, X., Macdonald, R. L., and Stitzel, J. A. (2004) *J. Neurochem.* **91,** 1138–1150
41. Chenna, R., Sugawara, H., Koike, T., Lopez, R., Gibson, T. J., Higgins, D. G., and Thompson, J. D. (2003) *Nucleic Acids Res.* **31,** 3497–3500
42. Schrödinger, LLC (2008) *Prime*, Version 2.0.110, Schrödinger, LLC, New York
43. Jacobson, M. P., Pincus, D. L., Rapp, C. S., Day, T. J., Honig, B., Shaw, D. E., and Friesner, R. A. (2004) *Proteins* **55,** 351–367
44. Phillips, J. C., Braun, R., Wang, W., Gumbart, J., Tajkhorshid, E., Villa, E., Chipot, C., Skeel, R. D., Kale, L., and Schulten, K. (2005) *J. Comput. Chem.* **26,** 1781–1802

45. Brooks, B. R., Bruccoleri, R. E., Olafson, B. D., States, D. J., Swaminathan, S., and Karplus, M. (1983) *J. Comput. Chem.* **4,** 187–217
46. Humphrey, W., Dalke, A., and Schulten, K. (1996) *J. Mol. Graph.* **14,** 33–38
47. Nielsen, J. S., Buczek, P., and Bulaj, G. (2004) *J. Pept. Sci.* **10,** 249–256
48. Jensen, A. A., Zlotos, D. P., and Liljefors, T. (2007) *J. Med. Chem.* **50,** 4616–4629
49. Gehrmann, J., Daly, N. L., Alewood, P. F., and Craik, D. J. (1999) *J. Med. Chem.* **42,** 2364–2372
50. Dutton, J. L., Bansal, P. S., Hogg, R. C., Adams, D. J., Alewood, P. F., and Craik, D. J. (2002) *J. Biol. Chem.* **277,** 48849–48857
51. Rogers, J. P., Luginbühl, P., Shen, G. S., McCabe, R. T., Stevens, R. C., and Wemmer, D. E. (1999) *Biochemistry* **38,** 3874–3882
52. Sasaki, T., Kobayashi, K., Kohno, T., and Sato, K. (2000) *FEBS Lett.* **466,** 125–129
53. Brust, A., and Tickle, A. E. (2007) *J. Pept. Sci.* **13,** 133–141
54. Bulaj, G., and Olivera, B. M. (2008) *Antioxid. Redox. Signal.* **10,** 141–155